Acta Crystallographica Section F
Structural Biology and Crystallization Communications
ISSN 1744-3091

Crystallization and preliminary X-ray diffraction studies of the abscisic acid receptor PYL3 and its complex with pyrabactin

Xingliang Zhang, Wei Wu and Zhongzhou Chen*

State Key Laboratory of Agrobiotechnology, College of Biological Sciences, China Agricultural University, Beijing 100193, People's Republic of China

Correspondence e-mail: chenzhongzhou@cau.edu.cn

Received 2 December 2011
Accepted 19 February 2012

Abscisic acid (ABA) modulates many developmental processes and responses to environmental stress. Recently, a family of pyrabactin resistance-like proteins (PYLs) in *Arabidopsis thaliana* were identified to be abscisic acid receptors. Although the 14 PYLs members share a similar sequence identity, they exhibit different responses toward pyrabactin. Apo-PYL3 is a dimer; however, its oligomeric state changes greatly on the addition of pyrabactin. Moreover, pyrabactin binds dimeric PYL3 in a nonproductive mode which prevents receptor activation and inhibition of PP2Cs. Here, the expression, purification and crystallization of apo-PYL3 and of PYL3 complexed with pyrabactin are reported. Diffraction data were optimized to 2.5 Å resolution for apo-PYL3 and to 1.83 Å resolution for PYL3–pyrabactin. The crystals of apo-PYL3 and PYL3–pyrabactin belonged to space groups $P4_12_12$ and $P2_12_12_1$, respectively.

1. Introduction

Abscisic acid (ABA) plays crucial roles in the regulation of seed germination, bud dormancy, plant growth and stomatal aperture, and in the response to abiotic stress (Cutler *et al.*, 2010; Raghavendra *et al.*, 2010). The ABA response allows the plant to adapt to developmental and environmental conditions. Therefore, understanding the details of the ABA pathway is one of the most important goals in plant research.

A recent major breakthrough in plant-hormone signalling was the identification of the ABA receptor. Firstly, the PYR1/PYLs family of proteins (hereafter referred to as PYLs) were identified to be ABA receptors by genetic and biochemical studies (Ma *et al.*, 2009; Park *et al.*, 2009; Santiago *et al.*, 2009). Soon after, structures of PYR1, PYL1 and PYL2 were determined by several research groups (Nishimura *et al.*, 2009; Melcher *et al.*, 2009; Yin *et al.*, 2009; Miyazono *et al.*, 2009). In addition, *in vitro* reconstitution of this signalling pathway was validated (Fujii *et al.*, 2009).

Although the PYLs-family members share a similar sequence identity, they exhibit different responses towards pyrabactin. Pyrabactin has been used as a selective ABA agonist/antagonist for the identification of PYLs-family proteins (Park *et al.*, 2009). The structures of apo PYR1, PYL1 and PYL2 and of their complexes with pyrabactin have recently been reported (Hao *et al.*, 2010; Peterson *et al.*, 2010; Melcher *et al.*, 2010). These structural investigations revealed that PYL2 exhibits a distinct response towards pyrabactin as an antagonist with an opened gate in a nonproductive mode which was incompatible with the binding of PP2Cs. In contrast, pyrabactin bound to PYL1 or PYR1 as an agonist with a closed gate in a productive mode which was favourable for the docking of PP2Cs and thus released PP2C-mediated inhibition of downstream proteins such as SnRK2 kinases. The SnRK2 kinases positively regulate ABA-induced gene expression by directly phosphorylating bZIP transcription factors (Hao *et al.*, 2010; Peterson *et al.*, 2010). Structural comparison between PYL1–pyrabactin or PYR1–pyrabactin and PYL2–pyrabactin indicated that the conformational change of the gate (Melcher *et al.*, 2009) in response to pyrabactin binding underlay the productive or nonproductive mode of PYLs. However, it is not clear that this mechanism is applicable to other ABA receptors.

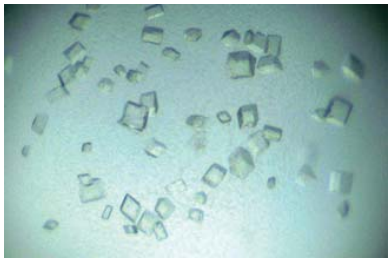

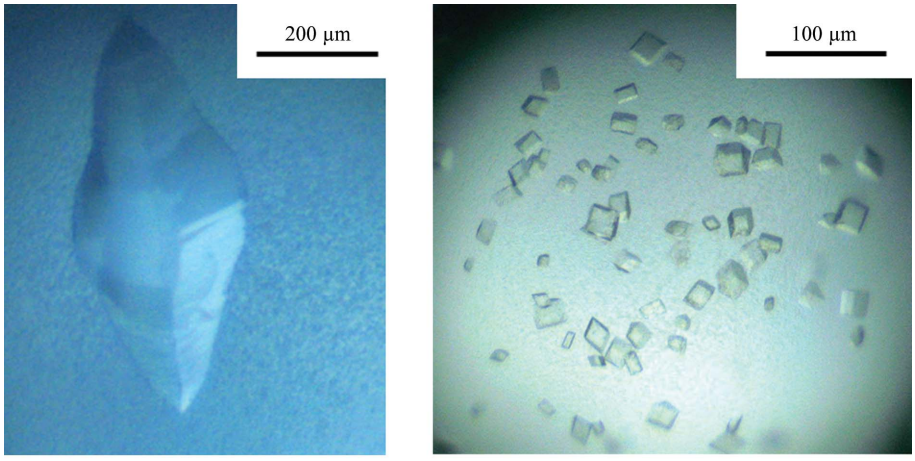

Figure 1
Typical crystals of apo-PYL3 (*a*) and PYL3–pyrabactin (*b*).

In a previous study, pyrabactin was shown to bind to PYL3 in a nonproductive mode using a Ser/Thr phosphatase assay system kit (Promega). In addition, PYL1, PYL2 and PYR1 were dimeric in solution with no obvious change upon binding pyrabactin. Interestingly, apo-PYL3 was also in a dimeric state. Size-exclusion chromatography and sedimentation-velocity experiments suggested that the molecular weight of pyrabactin-bound PYL3 decreased to 33.2 kDa, a value intermediate between those for monomeric and dimeric states (Yin *et al.*, 2009; Hao *et al.*, 2011). Therefore, whether the reported molecular mechanisms for pyrabactin binding are applicable to PYL3 remains unclear. These questions triggered our interest in elucidating the mechanism of the response of PYL3 to pyrabactin. Here, crystals of apo-PYL3 and PYL3–pyrabactin were successfully obtained and X-ray data were collected to 2.5 and 1.83 Å resolution, respectively.

2. Materials and methods

2.1. Protein expression

PYL3 (AT1G73000.1; residues 1–209) and a number of truncated fragments were amplified from the *Arabidopsis thaliana* cDNA library. The fragments were inserted into the *Bam*HI/*Xho*I sites of the pGEX-4T-2 vector (GE), in which the thrombin recognition site was replaced by a tobacco etch virus (TEV) protease recognition site. The recombinant plasmids were transformed into *Escherichia coli* strain JM109 cells, which were selected using ampicillin. The target gene sequences of positive colonies were verified by DNA sequencing. The correct plasmids were transformed into *E. coli* strain BL21 (DE3) (Novagen) for protein expression.

BL21 (DE3) cells transformed with PYL3 recombinant plasmid were incubated in 5.0 ml Luria–Bertani (LB) medium at 310 K overnight. The incubated cells were then transferred into 1.0 l LB medium at 310 K supplemented with 50 mg ml^{-1} ampicillin. When the absorbance of the cell culture at 600 nm (OD_{600}) reached 0.8, 0.1 m*M* isopropyl β-D-1-thiogalactopyranoside (IPTG) was added to induce expression for an additional 20 h at 293 K.

2.2. Protein purification

The cells were harvested by centrifugation at 4000 rev min^{-1} for 15 min, resuspended in lysis buffer (20 m*M* Tris–HCl pH 8.0, 150 m*M* NaCl, 1 m*M* DTT; buffer *A*) and lysed by sonication. The lysate was centrifuged at 20 000 rev min^{-1} for 20 min and the supernatant was filtrated using a 0.45 µm filter membrane to remove cell debris and other impurities. The supernatant was then applied onto glutathione Sepharose resin (GE Healthcare) and washed three times with a 20-fold bed volume of buffer *A*. 0.5 mg TEV protease was added to the resin to excise the GST tag (Supplementary Fig. S1*a*[1]). A further purification step was performed by size-exclusion chromatography (Superdex 200, GE Healthcare) equilibrated with buffer *A* (Supplementary Fig. S1*b*[1]). The final concentration of apo-PYL3 was 10–20 mg ml^{-1} in buffer *A* containing 2 m*M* tris(2-carboxyethyl)-phosphine. The freshly purified protein was immediately used in crystallization trials.

To obtain a homogeneous complex of PYL3–pyrabactin, pyrabactin (Sigma) was dissolved in DMSO to produce a 100 m*M* stock solution. Pyrabactin was then added to freshly purified PYL3 (residues 21–209) protein from size-exclusion chromatography to a final concentration of 0.5 m*M*, which was sufficient for PYL3 binding. After overnight incubation on ice, the mixture was further purified by size-exclusion chromatography to remove excess pyrabactin.

2.3. Crystallization

Initial crystallization trials were performed at room temperature using the sitting-drop vapour-diffusion method. The crystallization conditions used were from commercial crystallization kits (Hampton Research and Emerald BioStructures). The crystallization drop was composed of 1.0 µl well solution and 1.0 µl freshly purified apo-PYL3 protein or PYL3 complexed with pyrabactin and was equilibrated against 400 µl well solution. The crystals obtained from the initial crystallization trials were further refined by the hanging-drop vapour-diffusion method. Drops consisting of equal volumes (1.0 µl) of protein and well solution were equilibrated against 500 µl reservoir solution. In order to improve the crystal diffraction resolution, the cover slips with crystals were transferred gradually onto wells with a higher precipitant concentration. After dehydration, the crystals were transferred into well solution containing 30% glycerol as a cryoprotectant and flash-cooled in liquid nitrogen before data collection.

[1] Supplementary material has been deposited in the IUCr electronic archive (Reference: FT5019).

Table 1
Data-collection and processing statistics.

Values in parentheses are for the highest resolution shell.

	Apo-PYL3	PYL3–pyrabactin
Wavelength (Å)	1.0000	1.0000
Space group	$P4_12_12$	$P2_12_12_1$
Resolution (Å)	50–2.50 (2.54–2.50)	50–1.83 (1.86–1.83)
Unit-cell parameters (Å, °)	$a = b = 86.96$, $c = 154.12$, $\alpha = \beta = \gamma = 90$	$a = 53.63$, $b = 67.53$, $c = 109.08$, $\alpha = \beta = \gamma = 90$
R_{merge}† (%)	6.5 (87.4)	8.7 (52.9)
$\langle I/\sigma(I)\rangle$	75.9 (2.6)	29.7 (3.0)
Mosaicity (°)	0.487	0.644
Completeness (%)	99.3 (100.0)	98.4 (68.1)
Multiplicity	13.4 (9.0)	12.8 (5.4)

† $R_{merge} = \sum_{hkl}\sum_i |I_i(hkl) - \langle I(hkl)\rangle| / \sum_{hkl}\sum_i I_i(hkl)$, where $I_i(hkl)$ is the ith observed intensity of reflection hkl and $\langle I(hkl)\rangle$ is the average intensity over symmetry-equivalent measurements.

2.4. Data collection and processing

A high-resolution data set for apo-PYL3 was collected from a single crystal at 100 K on beamline NE3A at the Photon Factory (KEK). PYL3–pyrabactin data were collected on beamline 1W2B at the Beijing Synchrotron Radiation Facility (BSRF). The CCD detector was fixed at a distance of 180 and 250 mm for apo-PYL3 and PYL3–pyrabactin, respectively. The X-ray wavelength was 1.00 Å. Data collection from the crystals was performed using an angular range of 180° (apo-PYL3) or 360° (PYL3–pyrabactin), with an oscillation step of 1.0° and an exposure time of 0.5 s. All data were integrated and scaled with the *HKL*-2000 suite of programs (Otwinowski & Minor, 1997). Data-collection statistics are summarized in Table 1.

3. Results and discussion

Apo-PYL3 protein (residues 1–209) was concentrated to 20 mg ml^{-1} for crystallization. Many crystal nuclei appeared after 2 d in a 2 µl droplet at 291 K. The well solution consisted of 2.3 *M* ammonium sulfate, 0.1 *M* bis-tris propane pH 8.25. To reduce the formation of crystal nuclei, the protein sample and well solution supplemented with 10% glycerol were ultracentrifuged at 20 000 rev min^{-1} for 1 h and were immediately used in crystallization trials. After 3 d growth without any interference, very large crystals of apo-PYL3 were obtained, with one or two crystals in the droplet (Fig. 1*a*). However, the surface of the crystals was not smooth, probably owing to crystal-packing imperfections, which would be consistent with the very low diffraction resolution of these crystals. After extensive efforts involving testing hundreds of crystals and continuous dehydration with a final concentration of 30% glycerol in the well solution (Heras & Martin, 2005), the best crystal diffracted to 2.5 Å resolution and belonged to space group $P4_12_12$ (Fig. 2*a*). There were two PYL3 protomers in the asymmetric unit (Table 1).

Full-length PYL3 and a number of truncated fragments were purified in the presence of pyrabactin and subsequently screened for crystals of the protein–ligand complex. However, only one fragment of PYL3 (residues 21–209) successfully formed a complex crystal. Mass-spectrometric analysis of the complex crystal showed that it contained pyrabactin (Supplementary Fig. S2). To improve the crystal quality, pyrabactin–PYL3 (residues 21–209) was concentrated to 20 mg ml^{-1}. PYL3–pyrabactin complex crystals were obtained using a well buffer consisting of 1.7 *M* ammonium sulfate, 0.1 *M* sodium cacodylate pH 6.3, 0.2 *M* NaCl. The crystals were relatively small, but their edges and corners were very sharp and regular (Fig. 1*b*). The diffraction intensity of PYL3–pyrabactin also demonstrated that the crystal packing was very ordered. The best crystal diffracted to 1.83 Å resolution and belonged to space group $P2_12_12_1$ (Fig. 2*b*). There were two PYL3–pyrabactin molecules in the asymmetric unit (Table 1).

A dramatic change in crystal appearance between apo-PYL3 and PYL3–pyrabactin was observed. Pyrabactin binds to PYL3 in a nonproductive mode which prevents receptor activation and is incompatible with the binding of PP2Cs. The results of size-exclusion chromatography and sedimentation equilibrium showed that a

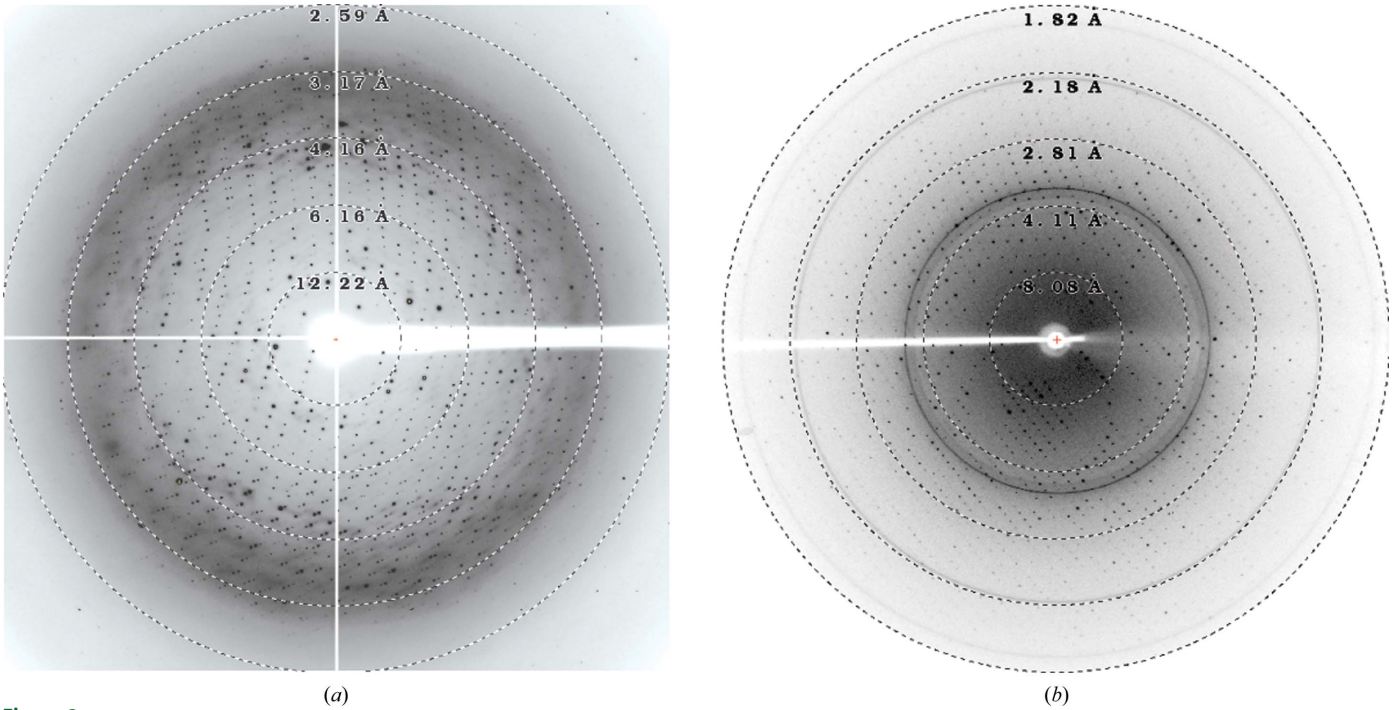

(*a*) (*b*)

Figure 2
X-ray diffraction images from crystals of apo-PYL3 (*a*) and PYL3–pyrabactin (*b*).

conformational rearrangement of PYL3 is triggered by the binding of pyrabactin. Based on the fact that PYR1 and PYL1–2 are dimers whereas PYL4–10 are monomers in solution with or without pyrabactin (Hao *et al.*, 2011), this may imply a novel binding mode between pyrabactin and PYL3. Structure determinations and *in vitro* biochemical experiments are currently in progress.

The project was supported by the National Basic Research Program of China (973 Program; 2011CB965304 and 2009CB825501), the National Natural Science Foundation of China (30870494 and 31070664) and the Fok Ying Tung Education Foundation (121025).

References

Cutler, S. R., Rodriguez, P. L., Finkelstein, R. R. & Abrams, S. R. (2010). *Annu. Rev. Plant Biol.* **61**, 651–679.
Fujii, H., Chinnusamy, V., Rodrigues, A., Rubio, S., Antoni, R., Park, S.-Y., Cutler, S. R., Sheen, J., Rodriguez, P. L. & Zhu, J.-K. (2009). *Nature (London)*, **462**, 660–664.
Hao, Q., Yin, P., Li, W., Wang, L., Yan, C., Lin, Z., Wu, J. Z., Wang, J., Yan, S. F. & Yan, N. (2011). *Mol. Cell*, **42**, 662–672.
Hao, Q., Yin, P., Yan, C., Yuan, X., Li, W., Zhang, Z., Liu, L., Wang, J. & Yan, N. (2010). *J. Biol. Chem.* **285**, 28946–28952.
Heras, B. & Martin, J. L. (2005). *Acta Cryst.* D**61**, 1173–1180.
Ma, Y., Szostkiewicz, I., Korte, A., Moes, D., Yang, Y., Christmann, A. & Grill, E. (2009). *Science*, **324**, 1064–1068.
Melcher, K. *et al.* (2009). *Nature (London)*, **462**, 602–608.
Melcher, K., Xu, Y., Ng, L.-M., Zhou, X. E., Soon, F.-F., Chinnusamy, V., Suino-Powell, K. M., Kovach, A., Tham, F. S., Cutler, S. R., Li, J., Yong, E.-L., Zhu, J.-K. & Xu, H. E. (2010). *Nature Struct. Mol. Biol.* **17**, 1102–1108.
Miyazono, K., Miyakawa, T., Sawano, Y., Kubota, K., Kang, H.-J., Asano, A., Miyauchi, Y., Takahashi, M., Zhi, Y., Fujita, Y., Yoshida, T., Kodaira, K.-S., Yamaguchi-Shinozaki, K. & Tanokura, M. (2009). *Nature (London)*, **462**, 609–614.
Nishimura, N., Hitomi, K., Arvai, A. S., Rambo, R. P., Hitomi, C., Cutler, S. R., Schroeder, J. I. & Getzoff, E. D. (2009). *Science*, **326**, 1373–1379.
Otwinowski, Z. & Minor, W. (1997). *Methods Enzymol.* **276**, 307–326.
Park, S.-Y. *et al.* (2009). *Science*, **324**, 1068–1071.
Peterson, F. C., Burgie, E. S., Park, S.-Y., Jensen, D. R., Weiner, J. J., Bingman, C. A., Chang, C. E., Cutler, S. R., Phillips, G. N. & Volkman, B. F. (2010). *Nature Struct. Mol. Biol.* **17**, 1109–1113.
Raghavendra, A. S., Gonugunta, V. K., Christmann, A. & Grill, E. (2010). *Trends Plant Sci.* **15**, 395–401.
Santiago, J., Rodrigues, A., Saez, A., Rubio, S., Antoni, R., Dupeux, F., Park, S.-Y., Márquez, J. A., Cutler, S. R. & Rodriguez, P. L. (2009). *Plant J.* **60**, 575–588.
Yin, P., Fan, H., Hao, Q., Yuan, X., Wu, D., Pang, Y., Yan, C., Li, W., Wang, J. & Yan, N. (2009). *Nature Struct. Mol. Biol.* **16**, 1230–1236.